UNIVERSIDADE FEDERAL DE UBERLÂNDIA
FACULDADE DE ENGENHARIA MECÂNICA
GRADUAÇÃO EM ENGENHARIA AERONÁUTICA

VINICIUS FERRO JACÓ MORETTO

STUDY OF THE NOISE AND AERODYNAMICS OF A PROPELLER USED IN DRONES BY APPLYING A LOW-FIDELITY METHOD

UBERLÂNDIA - MG
APRIL, 2022

UNIVERSIDADE FEDERAL DE UBERLÂNDIA
FACULDADE DE ENGENHARIA MECÂNICA
GRADUAÇÃO EM ENGENHARIA AERONÁUTICA

Vinicius Ferro Jacó Moretto

STUDY OF THE NOISE AND AERODYNAMICS OF A PROPELLER USED IN DRONES BY APPLYING A LOW-FIDELITY METHOD

Bachelor thesis submitted to the Undergraduate's Course of Aeronautical Engineering of Universidade Federal de Uberlândia, as a partial requirement for the bachelor's degree in Aeronautical Engineering.

Advisor: Prof. Dr. Tobias Souza Morais

Uberlândia - MG

April, 2022

Vinicius Ferro Jacó Moretto

STUDY OF THE NOISE AND AERODYNAMICS OF A PROPELLER USED IN DRONES BY APPLYING A LOW-FIDELITY METHOD

Bachelor thesis submitted to the Undergraduate's Course of Aeronautical Engineering of Universidade Federal de Uberlândia, as a partial requirement for the bachelor's degree in Aeronautical Engineering. Approved by:

Prof. Dr. Tobias Souza Morais
Faculdade de Engenharia Mecânica
Universidade Federal de Uberlândia

Prof. Dr. Odenir de Almeida
Faculdade de Engenharia Mecânica
Universidade Federal de Uberlândia

Prof. Dr. João Marcelo Vedovotto
Faculdade de Engenharia Mecânica
Universidade Federal de Uberlândia

Uberlândia - MG
April, 2022

ACKNOWLEDGMENT

First of all, I would like to thank my internship tutor, Mr. Ashkan Zaker, who helped me and taught me a lot throughout my work. I extend my thanks to the team members I worked with, in particular Mr. Jean-Philippe Gruau and Mr. Thierry Gachon the engineers who advised me throughout my internship, sharing their experiences, which was extremely important and beneficial to me.

With the same gratitude, I would like to thank my supervisor Tobias Souza Morais for his support, advice and guidance in my work, my English teacher Marina Furtado Mello for her advice with writing the paper and Giuliano Gardolinski Venson, coordinator of the aeronautical engineering graduation.

I also would like to thank Messrs. Olivier Vandamme, Mohamed Smahi, Hervé Lehmann, Abdollah El Aidi, Jean Fauconnier, and Rishvan Shaik-Madarsa for the engineers in training whose help was invaluable in carrying out this work.

In addition, I would like to thanks all my friends for all help, advice and wisdom. Finally, I thank my family, especially my father José Claudio Moretto, my mother Francislaine Ferro Jaco Moretto and my sister Laura Ferro Jaco Moretto who always supported and advised me.

RESUMO

O ruído gerado por drones multirotores é uma das barreiras para a intensa exploração desses equipamentos. Em virtude disso, estudos aeroacústicos foram realizados para estimar e reduzir a poluição sonora. As principais estratégias de simulação para realizar esses estudos são normalmente associadas a complexos e custosos modelos computacionais, o que não são adaptadas às fases iniciais do projeto de hélices. Assim, uma metodologia adaptada a esta etapa de projeto é apresentada neste trabalho. Para isto, o modelo Vortex Lattice foi utilizado para a predição de performance aerodinâmica das hélices, e a analogia aeroacústica de Ffowcs-Williams e Hawkings para os cálculos acústicos. Com o objetivo de tornar isto possível, os softwares OpenVSP e PSU-WOPWOP foram utilizados. Para avaliar a metodologia, análises sobre a qualidade de discretização geométrica das hélices, bem como os parâmetros temporais associados a simulação foram realizados. Além disso, um estudo para a validação dos dados aerodinâmicos e aeroacústico foi realizado, comparando os resultados calculados pela metodologia com dados experimentais disponíveis na literatura. Concluiu-se que o nível de pressão sonora global (overall sound pressure level) observado é subestimado em relação ao experimento, entretanto o nível sonoro em frequências específicas, como a frequência de passagem de pá, possui uma boa correlação. A metodologia foi ainda acoplada a um algoritmo de otimização diferencial para permitir a otimização da geometria das pás, objetivando a redução do ruído gerado.

Palavras-chave: Ruído, drones, multirotores, hélice, Vortex Lattice, Ffowcs-Williams e Hawkings, acústica, aeroacustica, aerodinâmica, OpenVSP, PSU-WOPWOP, simulação, evolução diferencial, otimização.

ABSTRACT

The noise generated by multirotor drones is one of the barriers to an intense exploration of these equipments. For this, aeroacoustics studies are carried out to predict and reduce noise pollution. The main simulation strategies to perform these studies are usually associated with a heavy Computational Fluid Dynamics (CFD) model, which is not adapted for the preliminary phase of propeller design. Thus, a methodology to be applied in this phase of the project is proposed in this work. In it, the Vortex Lattice Method was used for aerodynamic prediction and the acoustic analogy of Ffowcs-Williams and Hawkings for acoustic calculation. To make it possible, OpenVSP and PSU-WOPWOP software were used. To evaluate the methodology, analyses about the spatial and temporal discretization, and number of revolutions simulated were performed. In addition, an aerodynamic and acoustic validation study was carried out, comparing the results with experimental data, where the overall sound pressure level is underestimated, but the sound pressure level at blade passage frequency is well correlated. The methodology was also associated with a differential evolution algorithm to optimize the blade geometry reducing noise pollution.

Keywords: Noise, drones, multirotors, propeller, Vortex Lattice, Ffowcs-Williams and Hawkings, acoustics, aeroacustics, aerodynamics, OpenVSP, PSU-WOPWOP, simulation, differential evolution, optimization.

RESUMÉ

Le bruit généré par les drones multi-rotors est l'un des contraintes pour une exploration intense de ces équipements. Pour cela, des études aéro-acoustiques sont réalisées afin de prévoir et réduire la nuisance sonore. Les principales stratégies de simulation pour réaliser ces études sont généralement associées à un lourd modèle de dynamique des fluides numérique (CFD), qui n'est pas adapté à la phase préliminaire de conception des hélices. Ainsi, une méthodologie pour être appliquée dans cette phase du projet est proposée dans ce travail. Ici, la méthode « Vortex Lattice » a été utilisée pour la prédiction aérodynamique et l'analogie acoustique de Ffowcs-Williams et Hawkings pour le calcul acoustique. Pour rendre cela possible, les logiciels OpenVSP et PSU-WOPWOP ont été utilisés. Pour évaluer la méthodologie, des analyses sur la discrétisation spatiale et temporelle et le nombre de révolutions simulées ont été effectuées. De plus, une étude de validation aérodynamique et acoustique a été réalisée, comparant les résultats aux données expérimentales, où le *overall sound pressure level* est sous-estimé, mais le niveau sonore à la fréquence de passage des pales est bien corrélé. La méthodologie a également été associée à un algorithme d'évolution différentielle pour optimiser la géométrie des pales afin de réduire les nuisances sonores.

Mots clés : Bruit, drones, multi-rotors, hélice, Vortex Lattice, Ffowcs-Williams et Hawkings, acoustique, aéroacoustique, aérodynamique, OpenVSP, PSU-WOPWOP, simulation, évolution différentielle, optimisation.

LIST OF FIGURES

LIST OF TABLES

LIST OF ABREVIATIONS AND ACRONYMS

c	Sound speed in quiescent medium, m/s
CL_i	Design lift coefficient
CP	Power coefficient
CQ	Torque coefficient
CT	Thrust coefficient
D	Propeller diameter, m
d	Distance between observer and source, m
f	Generalized function
$H(f)$	Heaviside function
J	Advance ratio
l_i	Components of local force intensity that act on the fluid ($P_{ij}n_j$), Pa
M	Mach number of source
M_r	Mach number of source in radiation direction
n_i	Normal Vector
n	Revolutions per second, s^{-1}
p'	Acoustic pressure, Pa
P_{ij}	Compressive stress tensor, Pa
p'_L	Loading pressure, Pa
p'_T	Thickness pressure, Pa
r	Local propeller radius , m
R	Propeller radius, m
t	Time Variable, s
T	Propeller Thrust,N
T_{ij}	Lighthill stress tensor
U_∞	Free-stream velocity, m/s
U_n	Redefined “velocity” vector for an impermeable surface, m/s
u_n	Normal velocity of the fluid, m/s
v_n	Normal velocity of the blade surface, m/s
x_i	Spatial Variable,m

$\Box^2$	Wave operator, $\Box^2 = [(1/c^2)(\partial^2/\partial t^2)] - \nabla^2]$
$\delta(f)$	Dirac delta function
Γ	Horseshoe Vortex intensity
ϕ	Velocity potential
ρ'	Density fluctuation, kg/m^{-3}
ρ_0	Density of medium, kg/m^{-3}

BEMT	Blade Element Theory
BPF	Blade Passage Frequency, Hz
CAD	Computer-aided design
CFD	Computational Fluid Dynamics
DES	Detached Eddy Simulation
DNA	Deoxyribonucleic Acid
DNS	Direct Numerical Simulation
FEM	Finite Element Method
FW-H	Ffowcs-Williams and Hawkings
ITERMAX	Maximum number of iterations
LES	Large Eddy Simulation
MAV	Micro air vehicle
NVLM	Non-linear Vortex Lattice Method
OASPL	Overall Sound Pressure Level, dB
R&D	Research & Development
RPM	Rotations per minute
SPL	Sound pressure level, dB
VLM	Vortex Lattice Method

SUMMARY

1 INTRODUCTION

In the world around us, there are a big number of sources that produce sounds and noises, as a conversation, an airplane or even the functioning of the human body. It is possible to classify the sound wave in two different ways: when that wave is desired, as a music played in a concert, we name it as sound, but if this sound wave is disturbing and undesired, we call it “noise”.

There is a strong link between human and animal health and noise, so the sources with high sound level need to be avoided. As a consequence, some regulations were developed to control and limit noise pollution, which enables a technological evolution adapted to human health. The aeronautical and automotive sectors are both impacted by these regulations and in some cases, as example, some models of planes are banned from circulating in the vicinity of airports close to cities as a consequence of noise pollution. In recent years, we have seen a growing demand for unmanned micro air vehicle for military and civil applications. Also known as drones, these machines are useful for a wide range of missions, from recreation activities to delivery services. One of the types of drones is the multiple rotors, used thanks to the high performance in hovering and a good trade-off between stability and controllability. Despite their high versatility, a barrier to full exploration of this sector is noise pollution, where the biggest part is produced by the rotors. Thus, this study is focused on the development, understanding, and application of a methodology to estimate the noise of the low-Reynolds propellers.

Figure 1.1: Examples of using drones.

Source: www.urban-hub.com.

The noise produced by the propellers can be a consequence of several aeroacoustics phenomena. It can be produced by the movement of the propeller immersed in a fluid, by the influence of the wake produced by the rotor on itself, and by the interaction between the flow

induced by the propeller and the other structures of the drone. There are a large number of parameters that can influence the noise production in a drone, such as the blade geometry, the design of the arms that hold the motors, and the position of the propeller in relation to theses arms.

In addition to all behavior that influences aeroacoustics, studying the interaction between aerodynamics and acoustics it is not a simple task. Some aerodynamic phenomena that produce noise are complex to characterize, requiring heavy, expensive, and slow simulations to find a reliable result. In parallel with numerical studies, another option to know the aeroacoustics behavior of the propellers is to carry out experiments, but it requires specific equipment and acoustic rooms to minimize the influence of the error sources on the results. Beside all this, for a low-Reynolds regime, the viscous forces dominate the fluid momentum, which facilitates the boundary layer separation from the blade surface, which does not re-attach. Consequently, the noise generation mechanisms are different for small rotors compared to large rotors.

Due to all this complexity, the study of some aeroacoustic effects produced by a propeller requires a long calculation time and powerful computers, which makes its application in the early stages of design unfeasible. In these stages, notably, the preliminary and conceptual phases, the main interest is to compare different options of design, observing the gains and losses of one over the other. Thus, the speed to obtain the data can be prioritized to the detriment of the precision of the calculations. In this way, this work aims to present a methodology for aeroacoustic calculations using low-fidelity models with the objective of reducing the calculation time so that aeroacoustics studies can be applied to the initial phases of the propeller design.

For this methodology, the vortex lattice method is the low-fidelity theory chosen to perform aerodynamic simulations and the Ffowcs-Williams and Hawkings analogy for the aeroacoustic calculation. For this, the OpenVSP and PSU-WOPWOP software are linked and used in this work. This report will present the integration between the two software, as well as the aerodynamic and acoustic results of a propeller used in drones.

This work is the result of an internship program developed at Expleo Group, a company dedicated to consulting services in engineering, technology, quality, and management, working with partners ranging from the banking sector to the space and defense sector. The project took place in the company's research and development (R&D) core, more precisely in the Paris-FR agency.

1.1 OBJECTIVES

Since rotors are a major source of noise pollution from drones, their design has long been the subject of in-depth research. The conventional computational fluid dynamics (CFD) tool has helped engineers to optimize rotors. This tool, however, is an expensive method for such optimization in the early stages of design. In this way, the aim of the project is to develop a calculation methodology to estimate the aeroacoustic performance of rotors adapted to the preliminary phases of aeronautical projects, it means: with a reduced computation cost.

In order to answer this main objective, low-fidelity physical models are used to simulate rotors physics. For aerodynamic proposals, a vortex lattice method is used and for acoustics, Ffowcs-Williams and Hawkings analogy. The choice of both models will be explained later.

As we are looking at the conceptual and preliminary phase of a project, the interest is to produce a tool sensitive to capture acoustics and aerodynamics variations from geometric differences.

1.2 REPORT PLANNING

This current report will treat and present the methodology, results, and conclusions developed throughout the internship. In the first section, the subject is contextualized with the current position of the multirotor drones applications and the ambitions for the future, also, in the same section, a bibliographic review is detailed to locate this study among the scientific community. Thus, a methodology developed in this study for aerodynamic and aeroacoustics calculation is presented, followed by some cases for the validation of this methodology.

1.3 SUBJECT POSITION

Noise pollution has a direct impact on human health and behavior and can even influence the economy. This type of pollution is increasing in intensity due to urban concentration, the development and use of new technologies, such as the new modalities of the aeronautical sector like drones and eVtols.

The use of drones is becoming commonplace in everyday life. They have different applications ranging from aerial videography to parcel delivery. One of the main sources of sound from a drone are the propellers. Thus, the objective of this work is the aeroacoustic study of drone rotors.

2 BIBLIOGRAPHIC REVIEW

The aero-acoustics studies began in 1952 with the contributions of Lighthill [1], who sought to understand the noise radiation of jet engines in the period which commercial aviation began to implement these engines. Starting with the Euler's equations (mass, momentum, and energy conservation) and rewriting them into a kinematic wave equation form, he arrived at equations known as Lighthill's acoustic analogy [Eq. 1] (where $\rho^{'}$ represents the density fluctuation, c_o the speed of sound, t the time variable, x_i the spatial variable and T_{ij} the Lighthill's stress tensor).

$$\frac{\partial^2 \rho'}{\partial t^2} - c^2 \frac{\partial^2 \rho'}{\partial x_i^2} = \frac{\partial^2 T_{ij}}{\partial x_i \partial x_j} \tag{1}$$

Lighthill's also, manipulating the equations of analogy, demonstrated an "eighth-power law" where jet noise is proportional to the eighth power of jet's propulsion velocity ($I \propto u^8$). This knowledge was important to improve the jet engine design in order to reduce the noise radiation.

The previous analogy was used as a starting point for other acoustics analogies, whose objective was the aeroacoustic study in other applications. The Ffowcs-Williams and Hawkings analogy (FW-H) is an example of this [2]. In this analogy, the authors applied generalized mathematical functions to Lighthill's analogy to divide the domain into volumes and surfaces allowing the aero-acoustics modeling of moving objects. This modification enables the calculation of noise from rotors and propellers. FW-H is used in this project and a section is dedicated to give more details about the model.

Farassat [3] developed a time-domain integral formulation for FW-H analogy. Called Formulation 1A, it excludes the quadrupoles terms. Then, the acoustic pressure is calculated considering only the monopole and dipole terms, which physically represents the noise generated by the displacement of the fluid by the movement of an object (thickness noise), and the noise generated by the forces applied from the aerodynamic surface on the fluid (loading noise), respectively. This formulation is valid to rigid-body surface motion, but some modifications can be applied to simulate flexible structures. The equation [Eq. 2] determines the acoustic pressure (p') in function of thickness ($p_T^{'}$) and loading pressure ($p_L^{'}$).

$$p'(x,t) = p'_T(x,t) + p'_L(x,t) \tag{2}$$

Rotor noise sources can be divided into two categories [4]: deterministic and non-

deterministic. The deterministic sources produce a tonal noise spectrum, where periodic peaks can be observed at rotation frequency and harmonics. Brentner and Farassat in [5] identify four deterministic sources in a rotor: thickness noise, loading noise, blade vortex interaction noise (tip vortex from a first blade impacting the next), and high-speed impulsive noise (noise associated with the existence of a transonic flow in a part of the blade). On the other hand, non-deterministic sources (also known as broadband noise) produce a random sound signal generated by the interaction of the turbulent flow with the blade surface. Three broadband rotor noise sources are defined: turbulence ingestion noise [6] (noise due to ingestion of atmospheric turbulence), blade wake interaction noise [7] (noise due interactions between blade and rotor wake turbulence), and blade self-noise [8] and [9] (noise caused by the interaction of turbulent flow over the blade trailing edge). Figure 2.1 illustrates the noise radiation for the different sources in a rotor, and Figure 2.2 summarizes the noise sources produced by the propellers.

Figure 2.1: Rotor noise radiation.

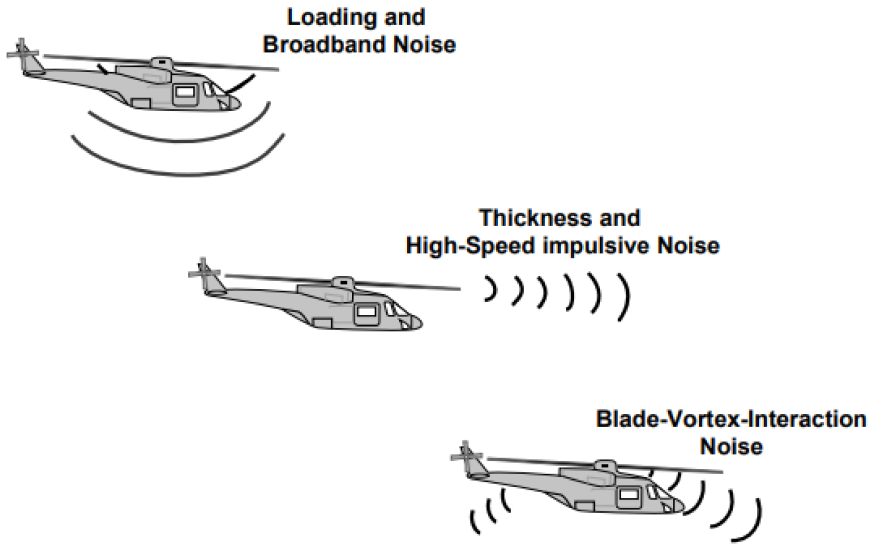

Source: K. S. Brentner and F. Farassat [5].

Figure 2.2: Schematic to summarize the noise sources of a propeller.

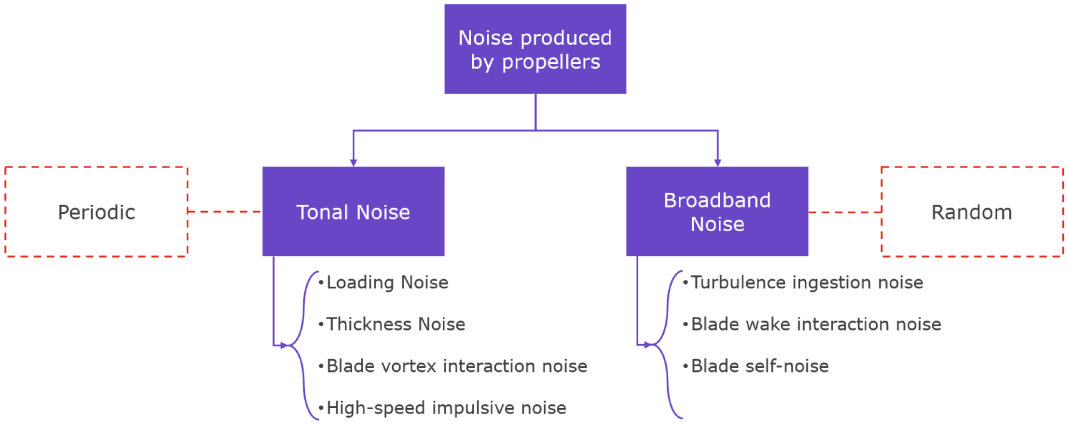

Source: Own authorship.

Based on FW-H analogy and Farassat's Formulation 1A, Brentner et al. [10] developed an acoustic solver capable to predict the noise radiation of a rotating object, noticeably propellers and rotors, named PSU-WOPWOP. As function of the formulation used in this solver, thickness and loading noise are predicted. The software also has a module to predict the broadband noise, where two models are available, the Robert Pegg method [11] and BPM method [8], propose by Thomas F. Brooks, D. Stuart Pope, and Michael A. Marcolini. As the solver needs to receive the aerodynamic data, it is possible to combine it with different calculation methodologies, such as CFD calculation or vortex lattice method.

In recent years, an interest to study the low Reynolds propeller instigated the production of scientific publications about this subject. Brand et al. [12] carried out a study to measure the geometric characteristics of commercial propellers commonly used in drone and model airplanes. In this same work, they did experiments with the propellers to measure the performance properties of each. A static (with no flow speed) and a dynamic experiment in a wind tunnel were performed. All these data acquired are available on a public database [13].

Zawodny et al. [4] investigated numerically and experimentally the hover performance and aeroacoustic results of two propellers geometries used in a micro air vehicle (MAV) rotor. In this study, they used the experimental data to validate a low-fidelity model based on Blade Element Theory (BEMT) and a high fidelity model where a Detached Eddy Simulation (DES) was performed. For the acoustic calculation, they used the FW-H analogy running the PSU-WOPWOP solver. In addition, they performed a semi-empirical model for the broadband noise prediction. The authors also developed a study about sound directivity, doing a comparison with the experimental results.

In [14] the same propellers studied in [4] are investigated using a non-linear vortex lattice method (NVLM) as the aerodynamic solver. This method allows to run unsteady simulation with a low-fidelity model, rather than BEMT simulations, able to calculate only steady solutions. A convergence with respect to spatial and temporal resolution is studied and a validation is performed, comparing the results with experimental data and high-fidelity calculation.

In the studies of Nana et al. [15] and later Serré et al. [16], a design optimization of a rotor was performed using BEMT, aiming to improve the aerodynamic performance and to reduce the noise radiation. For the acoustic model, FW-H and a statistical broadband noise were used. In the publication of Serré et al., the results of the optimization are presented, as well as an experimental validation.

3 METHODOLOGY

From the studies published by Lighthill in 1952, the methodologies for aeroacoustics calculation started to be developed and applied in engineering projects. Nowadays, new solutions and techniques of calculation are still under development by the scientific and industrial community, especially with the evolution of computational power. There are three main strategies for aeroacoustics simulation used currently:

- Direct CFD computation.
- Hybrid methods.
- Semi-empirical models.

The direct method consists of calculating in the same domain, the aerodynamic and aeroacoustic field. This option is, theoretically, the most accurate method, but also the most challenging. First, a compressible and unsteady CFD simulation is required. The greater the accuracy of aerodynamics results, the greater the accuracy of acoustic calculation, but this is associated with expensive computational methods such as Direct Numerical Simulation (DNS), Large Eddy Simulation (LES), and Detached Eddy Simulation (DES). Second, the aerodynamic field needs to be resolved for the entire aeroacoustic field, which in some cases increases the size of the aerodynamic domain, dramatically increasing the computational cost. The last challenge is about the numerical methods: normally the CFD numerical schemes are dissipative for stability proposals and can kill acoustic signals because the magnitude of hydrodynamic and acoustic pressure are different, also some aerodynamic and aeroacoustic boundary conditions are incompatible and, as consequence, it can induce unwanted acoustic wave reflections.

The hybrid method separates the aeroacoustic simulation into two steps. In a first moment, an aerodynamic unsteady simulation is performed, and then the CFD results are used as input to an acoustic simulation. A region of the aerodynamic domain is taken as a noise source and the acoustic wave radiated by it is propagated using a finite element method (FEM) or acoustic analogies (like Lighthill or Ffowcs-Williams and Hawkings analogies). The fact that the aerodynamic field does not need to be evaluated in the entire acoustic region allows a reduction in the size of the domains compared to direct simulations, which reduces the calculation cost. However, the accuracy of the results is still linked with the CFD simulation type. Despite the constraints, this strategy shows a good trade-off between efficiency and accuracy, which makes it an interesting option for industrial applications.

Figure 3.1 illustrates the difference between the two methods, for the direct method the aerodynamic calculation zone needs to be the same as acoustic zone. For the hybrid method, the acoustic domain can be larger than the aerodynamic zone.

Figure 3.1: Schematic to illustrate the direct (a) and hybrid acoustic methods (b).

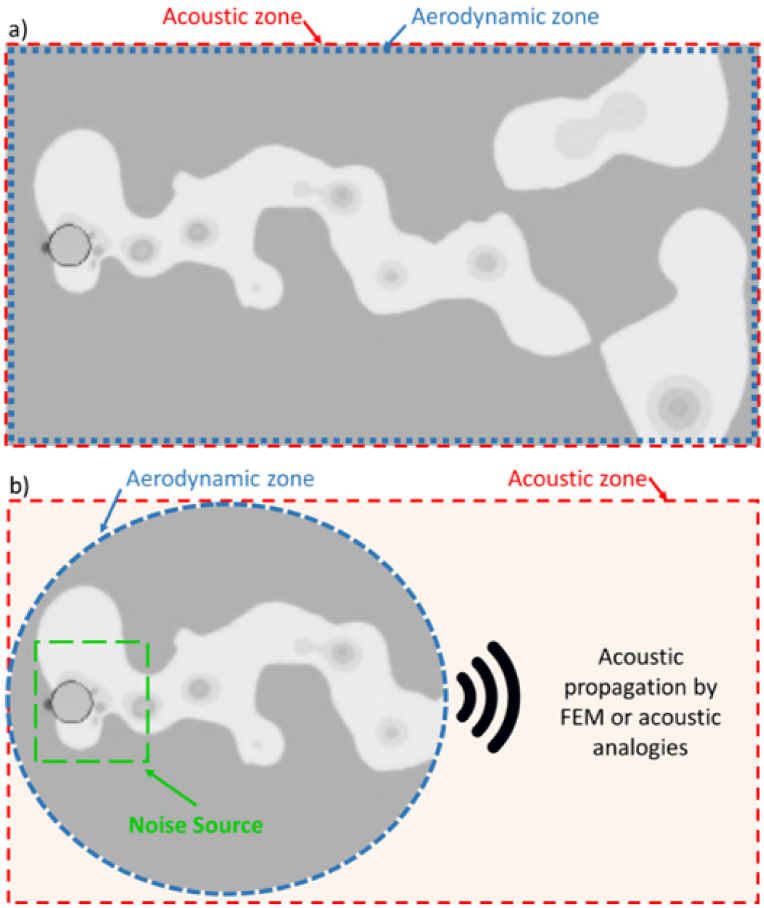

Source: Own authorship.

The semi-empirical models (SNGR) are based on experimental observation and because of that, it can be applied for specific cases. The advantage is that the method only needs the steady CFD simulation, which further reduces the computational cost.

Based on the previous strategies, the hybrid option seems the best choice for the aeroacoustic design of a low-Reynolds propeller. However, the usage of CFD simulation is not adapted for the preliminary stage of the project, where many geometries need to be evaluated and compared. At this work, the interest is to capture the differences between the geometries rather than a great precision in the results. For this reason, a methodology using the vortex lattice method (VLM) instead of CFD simulations is developed in this work. The next topic gives more details about the methodology.

3.1 HYBRID STRATEGY WITH VORTEX LATTICE METHOD

In order to develop a tool adapted to the preliminary phase of design, the methodology presented in Figure 3.2 is carried out. The starting point is to discretize the blade's geometry with some parameters, such as the repartition of chord, twist, and thickness. Thus, in this sense, OpenVSP is used: a geometric solver developed by NASA for preliminary and conceptual design in the aeronautical sector.

Figure 3.2: Flowchart of the methodology developed to design propellers and perform aerodynamics and aeroacoustics simulations.

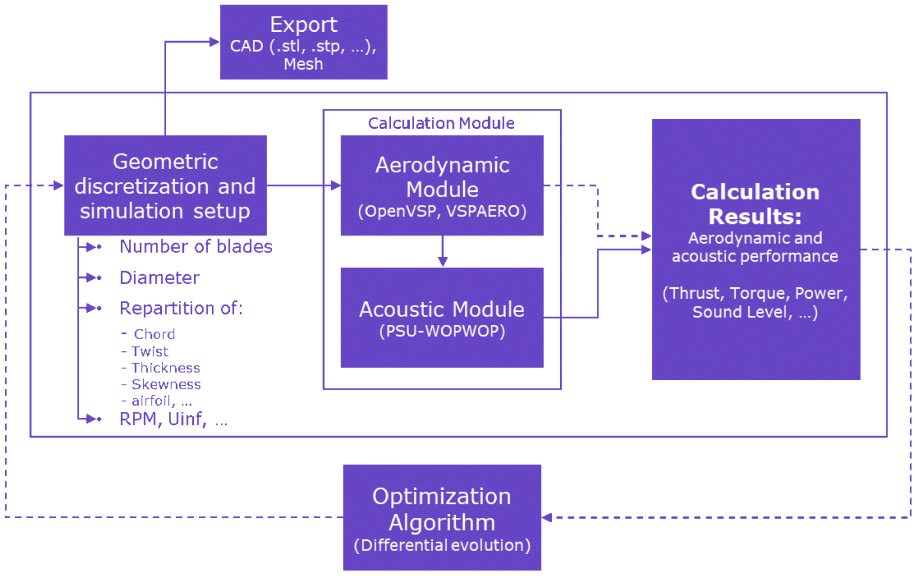

Source: Own authorship.

OpenVSP is a complete solver, which allows building geometries with relative complexity. It can be used not only for propeller and blade design, but also for the design of the entire aircraft, as is shown in the Figure 3.3. The interest in this software is also due to the possibility to export the geometries in CAD files format, which is appreciated for generating models for CFD simulation or 3D printing.

In addition to the geometric solver, OpenVSP proposes an aerodynamic module called VSPAERO. It is based on a low-fidelity method, whose objective is to propose a fast tool for preliminary aerodynamic prediction. There are two theories available, the panels' method and the vortex lattice method (VLM), but for propellers and rotors, the second one should be chosen. One of the advantages of this method is the ability to perform non-stationary simulations, which allows having results in a much shorter time than a high-fidelity method (forty minutes against eight hours to perform, in the same hardware setup, the same simulation using respectively the VLM and URANS $k-\omega$ SST). However, the VLM implemented in VSPAERO does not predict the non-linear aerodynamic effects, which restrict applications to medium and low angles of attack. The section 3.3 is dedicated to present the vortex lattice method.

Although OpenVSP is a feature-rich software, it has no acoustic solver implemented

Figure 3.3: Uber Elevate eCRM-002 made available as an example case by OpenVSP (a). Propeller APC 11x4.7 slow fly modeled on OpenVSP(b).

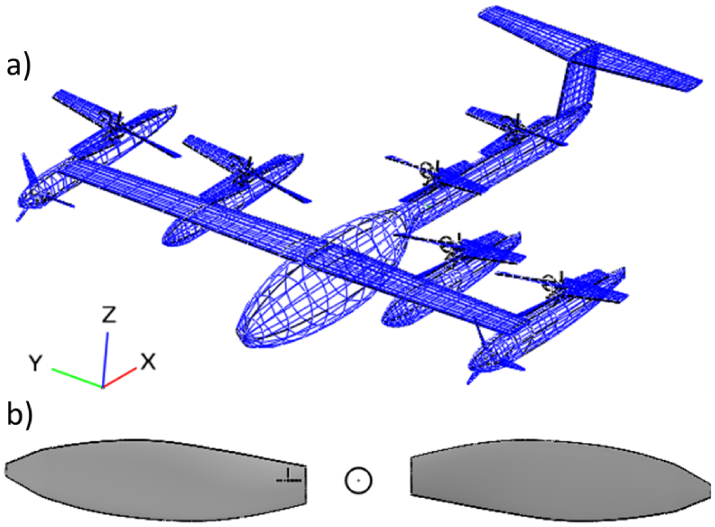

Source: Own authorship.

directly, but it can be linked with PSU-WOPWOP software, an acoustic solver developed for propellers and rotors noise prediction. To perform a simulation in PSU-WOPWOP, it is necessary to input the three files listed below. These files contain data about the propeller geometry and the aerodynamic forces. A specific data structure needs to be respected and hexadecimal format is used. This data structure is presented in chapter 7 of the software's user guide [10]. OpenVSP has a functionality to export files ready to be introduced on PSU-WOPWOP.

- 1D geometry file: the 3D geometry is compacted and converted in a 1D line where the loads are applied.
- Loading file: contains the loading vectors calculated by VSPAERO and applied under the previus line. These data are used for the loading noise calculation.
- Surface geometry file: contains the 3D geometry of the blade for thickness noise calculation. These data are inputted as a surface mesh, and the file contains the nodes of the elements and the normal vector.

As mentioned previously (in section 2), PSU-WOPWOP uses the FW-H analogy and Farassat Formulation 1A solution, which makes possible the prediction of the thickness and loading noise. As result, the solver can calculate the acoustic pressure in the temporal domain and the sound pressure level (SPL) in the frequency domain. It presents the contributions of each acoustic source (thickness and loading) and the total noise. It is possible to calculate the overall sound pressure level (OASPL) and generate audio files. These data are calculated at the position of a virtual microphone placed on the acoustic domain. Due to acoustic analogies and simplifications considered on the solution, the near field is not so well modeled, and the

receiver needs to be well positioned. The software also works with a change of base system and it enables the motion of surfaces and observers. It is possible then to simulate the passage of an airplane over an observer, for example.

A Python code was developed following the flowchart shown in the Figure 3.2 to integrate the geometric, aerodynamic, and acoustic solvers. The aim is to facilitate and accelerate the propeller modeling and the prediction of aerodynamic and aeroacoustic performance. The chapter 4 presents the results obtained with this methodology. A second objective was also to build a tool to be coupled to an optimization algorithm, presented in section 3.2.

3.2 METHODOLOGY FOR OPTIMIZATION

The python code containing the link between OpenVSP and PSU-WOPWOP was adapted to be coupled with an optimization algorithm based on differential evolution. The idea of the code is to vary the blade geometry, looking for the best combination for an objective function.

The flowchart presented in Figure 3.4 shows the structure of the optimizer. A base geometry is set, as well as the variation interval for the optimization parameters and the simulation condition. The differential evolution is a code that generates a population with several individuals, where each one consists of a vector containing the value for the geometric parameters that are varied. An analogy possible for this vector is human DNA, where the individual's characteristics are defined by it. The performance of all individuals is evaluated using OpenVSP and PSU-WOPWOP and an objective function is defined, using the results extracted from the model. This function is usually an equation that can mix the aerodynamic and acoustic results, as example the overall sound pressure level and the propeller torque. The characteristics of the best individuals are mixed and a new population is generated. There is also a mutation factor, to avoid the convergence to a local minimum. This procedure is repeated until reaching the convergence or the number max of iterations (itermax).

The interest is to perform an iso-thrust optimization to compare the acoustic performance under the same conditions. The rotation speed for the same thrust is different for each individual. Thus, a module was developed to search for the proper rotation speed, where the propeller is simulated for two pre-defined rotation speeds and the aerodynamic performance is evaluated. Then, a linear interpolation is done to determine the required rotation speed for the specified thrust. Typically, thrust has a quadratic dependence on rotation speed, however, to reduces the computational cost a linear approximation is made. In the tests performed, the relative error between the specified thrust and the real value calculated with a linear approximation was always less than 5%, but it depends on the two rotation speeds pre-determined.

Figure 3.4: Flowchart about the algorithm for acoustic optimization.

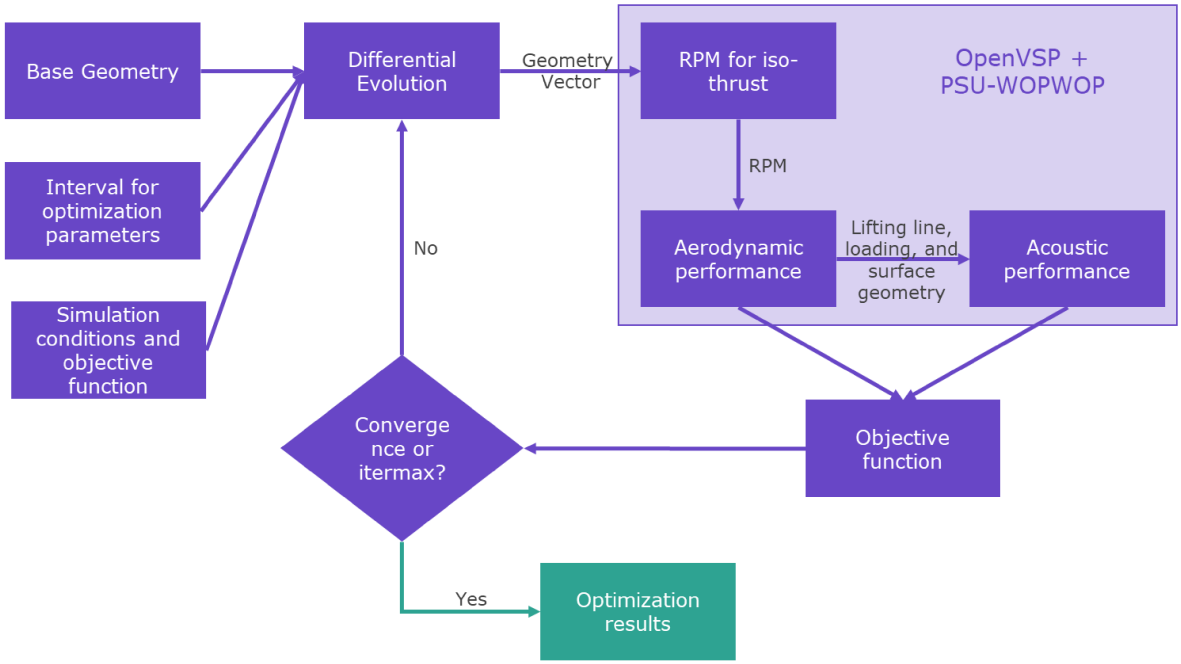

Source: Own authorship.

3.3 VORTEX LATTICE METHOD - VLM

The vortex lattice method is an aerodynamic approach classified as a low-fidelity method, where the assumptions of incompressible, inviscid, and irrotational flows are taken. In this methodology, the aerodynamic surface is discretized into two-dimensional panels on which Laplace equation [Eq. 3] for the velocity potential ϕ is solved. This equation is derived from Navier-Stokes equations, using the assumptions mentioned above.

Once the panels are defined, a horseshoe vortex of intensity Γ is placed on the surfaces and a control point is defined for each panel. This vortex induces a velocity across the calculation domain, which can be determined by applying the Biot and Savart's law [Eq. 4]. Then, the induced velocity is calculated for all control points, which allows defining a system of equations whose variable to be determined is the vortex intensity. This system is closed with the non-penetration condition at the blade surface and Kutta condition at the trailing edge. After solving the system and finding the intensity of all vortexes, the aerodynamic forces can be determined using the Kutta-Joukowski theorem.

Figure 3.5 illustrates the division of aerodynamic surfaces into panels and the horseshoe vortex. Also, it is shown the spatial variable used in Biot and Savart's law [Eq. 4].

$$\nabla^2\phi = \phi_{xx} + \phi_{yy} + \phi_{zz} = 0 \tag{3}$$

$$dV = \frac{\Gamma}{4\pi}\frac{dl \times r}{|r|^3} \tag{4}$$

Figure 3.5: Division of a wing into several panels and the representation of a horseshoe vortex. (b) Vortex filament and variables for the Biot and Savart's law, the velocity vector dV is perpendicular to the plane defined by the segment r and dl.

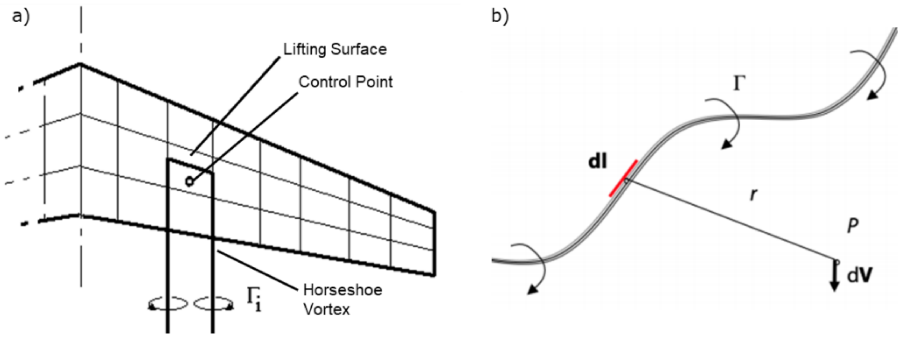

Source: Own authorship.

Despite the method's advantages, such as the computational cost and the possibility to performing non-stationary simulations, the VLM has some limitations. The solver implemented on OpenVSP is not able to run simulations for hover conditions because there is no free-stream velocity, and the software has problems to converge. In addition, the solver is linear and does not predict the non-linear aerodynamic effects, as a stall, which makes simulations at low free-stream difficult, as explained in section 4.6. Furthermore, the effect of thickness is not captured by VLM for aerodynamic analysis (but still impacts acoustic analysis).

Aerodynamic models that use potential equations, where the viscosity is neglected, may have difficulties in working with low Reynolds number. For this condition, the boundary layer is laminar, and it facilitates the separation of the boundary layer, what is not captured by these methods. As it is a potential method, VLM may have problems to work with very low-Reynolds (less than 10^5), but it was chosen because the propellers of interest in this work operate with Reynolds number greater than 90 000, and also for being a fast, consolidated and easy-to-use option.

Figure 3.6 shows the behavior of the lift coefficient as a function of angle of attack for a NACA-2412 airfoil. A linear characteristic is observed between the angle of attack of -8.75° and 10.75°. Outside this interval, non-linear effects are observed. This is due to the viscosity effects, which are not modeled in VSPAERO. In [14] a correction to consider the non-linear effects is applied to VLM and the aerodynamic and acoustic results for a case study are performed, but this correction is not considered in this work.

Figure 3.6: Linear and non-linear aerodynamics effects: Linear and non-linear aerodynamics effects.

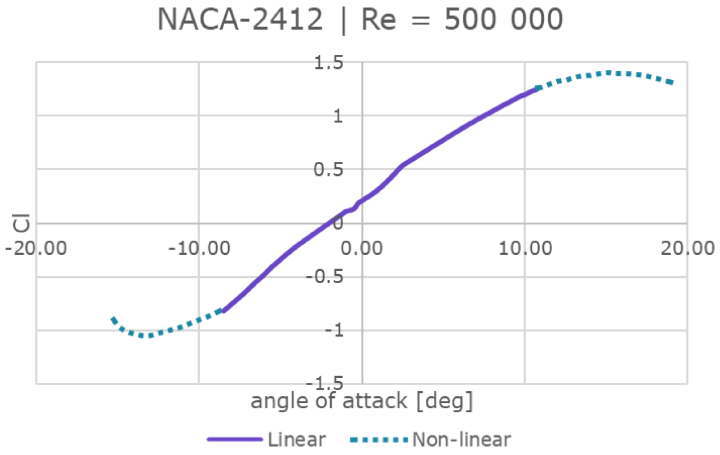

Source: Own authorship.

3.4 FFOWCS-WILLIAMS AND HAWKINGS AND FARASSAT FORMULATION 1A

Ffowcs-Williams and Hawkings is an extension of the Lighthill acoustic analogy, where they reformulated the Navier-Stokes equations using generalized functions [Eq. 5] to predict the noise of moving objects. The [Eq. 6] presents the differential form of the analogy. The three terms on the right-hand side of the FW-H equations are respectively the monopole ($\partial/\partial t$), dipole ($\partial/(\partial x_i)$) and quadrupole ($\partial^2/(\partial x_i \partial x_j)$). In this equation: $\Box^2$ is the wave operator, p' the acoustic pressure, ρ_0 density of medium, U_n redefined "velocity" vector for an impermeable surface, u_n normal velocity of the fluid, $\delta(f)$ Dirac delta function, P_{ij} compressive stress tensor, n_j normal vector, T_{ij} Lighthill stress tensor and $H(f)$ Heaviside function.

$$f = \begin{cases} > 0 \text{ Outside the surface} \\ = 0 \text{ On the surface} \\ < 0 \text{ Within the surface} \end{cases} \tag{5}$$

$$\begin{aligned} \Box^2 p'(x,t) = & \frac{\partial}{\partial t}\left\{\left[\rho_0 U_n + \rho\left(u_n - U_n\right)\right]\delta(f)\right\} \\ & - \frac{\partial}{\partial x_i}\left\{\left[P_{ij}\hat{n}_j + \rho u_i\left(u_n - U_n\right)\right]\delta(f)\right\} \\ & + \frac{\partial^2}{\partial x_i \partial x_j}\left[T_{ij} H(f)\right] \end{aligned} \tag{6}$$

Monopole, dipole, and quadrupole are acoustic sources with different directivity properties. For the monopole, sound is radiate equally in all directions as the noise generated by a small sphere with the radius expanding and contracting or a net flux of fluid. The dipole is formed by two monopoles with opposite phases and separated by a small distance, therefore, a

preferential radiation direction is observed. This source is normally produced by a force applied to the fluid. Two identical dipoles with opposite phases and separated by a small distance define a quadrupole. This type of acoustic source is associated with fluid shear stress and is a poor sound radiator for low-velocity flux, thus it is usually neglected in subsonic cases. Figure 3.7 illustrates the acoustic radiation for the three acoustic sources.

Figure 3.7: Acoustic radiation by a monopole, dipole, and quadrupole.

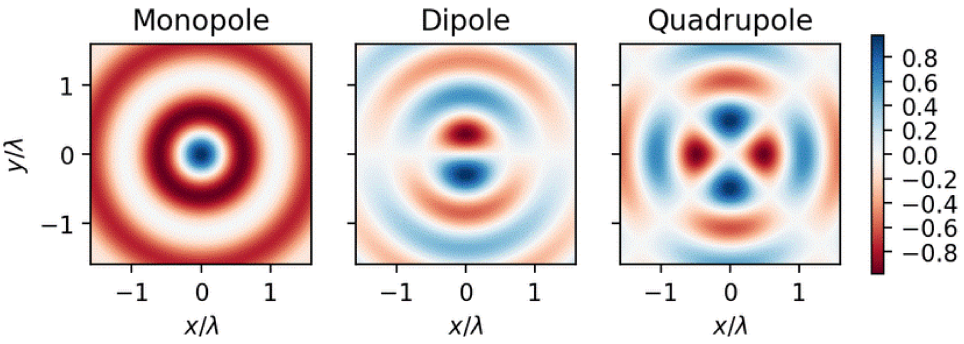

Source: J. Jordaan [17].

The generalized function f is implicit in the Dirac delta function $\delta(f)$ in the terms monopole and dipole, both surface sources. Generalized functions are, then, a mathematical device for dividing the domain into regions outside, on, and inside the surfaces. The quadrupole is, however, a volume term, and a Heaviside function $H(f)$ is used for dividing the domain into volumes inside and outside the acoustic surface, as presented in [Eq. 7].

$$H(f) = \begin{cases} 0 & (f < 0) \\ 1 & (f > 0) \end{cases} \tag{7}$$

A solution proposed by Farassat [3] and known as Formulation 1A is implemented on PSU-WOPWOP. It consists of an integral form solution of the FW-H equations. The quadrupole is neglected, and the acoustic pressure is determined by the remaining terms [Eq. 2], notably the monopole, which models the thickness noise, and the dipole, responsible for modeling the loading noise. The integral form of the acoustic pressure by thickness noise is present in [Eq. 8] and by loading noise in [Eq. 9]. The terms in the equations are: v_n normal velocity of the blade surface, d distance between observer and source, M_r mach number of source in radiation direction, c sound speed in quiescent medium, M mach number of source, and l_i components of local force intensity that act on the fluid ($P_{ij}n_j$).

$$4\pi p'_T(\mathbf{x},t) = \int_{f=0} \left[\frac{\rho_0 \left(\dot{v}_n + v_{\dot{n}}\right)}{d\left(1-M_r\right)^2} \right]_{\text{ret}} dS + \int_{f=0} \left[\frac{\rho_0 v_n \left(d\dot{M}_r + c\left(M_r - M^2\right)\right)}{d^2\left(1-M_r\right)^3} \right]_{\text{ret}} dS \tag{8}$$

$$
\begin{aligned}
4\pi p'_L(\mathbf{x},t) = & \frac{1}{c}\int_{f=0}\left[\frac{\dot{l}_r}{d\left(1-M_r\right)^2}\right]_{\text{ret}} dS + \int_{f=0}\left[\frac{l_r - l_M}{d^2\left(1-M_r\right)^2}\right]_{\text{ret}} dS \\
& + \frac{1}{c}\int_{f=0}\left[l_r\frac{d\dot{M}_r + c\left(M_r - M^2\right)}{d^2\left(1-M_r\right)^3}\right]_{\text{ret}} dS
\end{aligned}
\tag{9}
$$

On PSU-WOPWOP solver, the integrals are evaluated as discrete and derivates as difference equations. The subscript *ret* indicates that the terms are considered at the retarded time. The objects analysed are meshed, and the contribution of each mesh element is calculated and summed for a receiver placed in the domain.

A mathematical proof of the FW-H analogy is present in chapter 5 of [18].

4 ANALYSIS AND RESULTS

This section presents the analyses developed and the results obtained. Here, the objective is to understand the strengths and weaknesses of the methodology and the validity limit of the models. The analyses were performed using the code developed in this work, which integrates the aerodynamic and aeroacoustic solvers mentioned in the previous section. Thus, the analyses began with a convergence study about spatial and temporal discretization, and also the number of revolutions simulated. Once the ideal simulation parameters were known, a validation study was performed, comparing the aerodynamics and aeroacoustics results with data available in the literature. Then, a case to test the optimization code is described.

To carry out the studies of convergence and validation, the propeller APC 11x4.7 SF was used. Its geometric parameters are presented in the next topic.

4.1 APC 11x4.7 SF PROPELLER

This propeller is manufactured by APC Propellers® and the numbers 11 and 4.7 in the nomenclature indicate respectively, the diameter and pitch of the blades in inches. Also, the acronym "SF" means slow fly and indicates that this propeller was conceived for low-speed flights. Due to the size and performance specification, this propeller is mainly used in drones and model airplanes.

The interest in basing the study on this geometry is because this propeller can be used for drones and MAVs, the same applications on which this study focuses. Furthermore, there is a relatively reach literature about APC 11x4.7 SF, and it is possible to find the geometric discretization and aerodynamic and acoustic data.

The geometric discretization of this propeller can be found on UIUC Propeller Data Site [13], a database that contains the geometric discretization and wind tunnel measurements for about 140 propellers. On the website, is available the distribution of chord and twist angle of the blades, as is shown in Figure 4.1. However, other parameters are important for aerodynamics simulation, such as the cross-section airfoil, which is not available in the database. In this case, the manufacturer indicates the use of Eppler 63-type airfoil at the hub position and a Clark-Y type airfoil at the tip, with a linear transition between them. Other geometric parameters were fitted based on the images of the propeller. A preview of the propeller model creates on OpenVSP, as well as the front view of the propeller is shown in Figure 4.2. As shown in this figure, the hub region in the numerical model is not populated by any element and the absence

of elements in this region was not studied in this work. This may have some influence on the results and will be analyzed later, in the next stages of the study.

Figure 4.1: Chord and twist angle discretization for APC 11x4.7 SF.

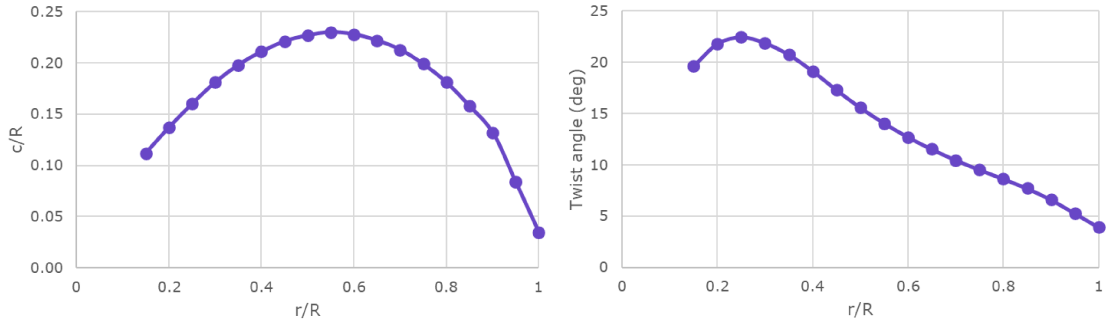

Source: Own authorship.

Figure 4.2: Comparison between the propeller modeled in OpenVSP (top) and front view of the real propeller (bottom).

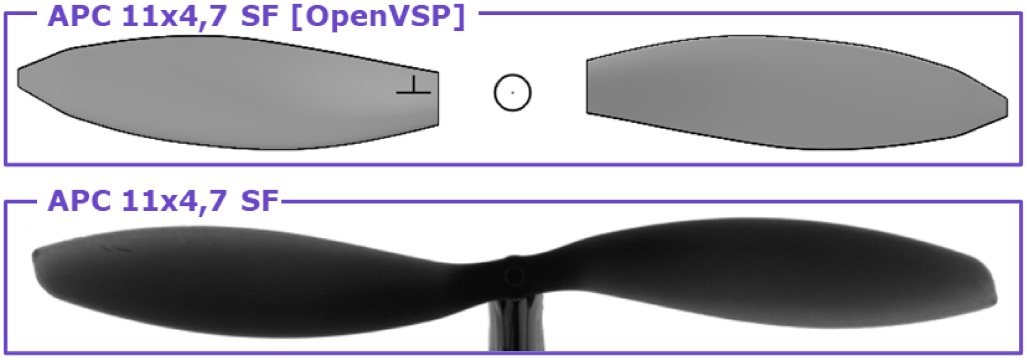

Source: Own authorship (top); J. Brandt et al. [13] (bottom).

4.2 Propeller Aerodynamic Coefficients

The aerodynamic coefficients are dimensionless values based on parameters such as force, speed, and length. The use of coefficients in dimensionless form is interesting, as this allows to compare different propellers' geometries and results obtained from different fluid conditions, such as temperature and density.

For propeller applications, the main coefficients are listed in the Table 4.1 and the dimensional parameters in Table 4.2.

Table 4.1: Propeller aerodynamic coefficients.

Advance Ratio	$J = \frac{U_\infty}{(nD)}$
Thrust Coefficient	$CT = \frac{T}{(\rho n^2 D^4)}$
Power Coefficient	$CP = \frac{P}{(\rho n^3 D^5)}$
Torque Coefficient	$CQ = \frac{Q}{(\rho n^2 D^5)}$

Source: Own authorship.

Table 4.2: Propeller performance parameters.

U_∞	Free-stream velocity	m/s
n	Revolutions per second	$s^{(-1)}$
D	Propeller diameter	m
T	Propeller thrust	N
P	Propeller power	W
Q	Propeller torque	$N.m$
ρ	Air density	kg/m^3

Source: Own authorship.

4.3 SPATIAL DISCRETIZATION CONVERGENCE

In OpenVSP, there are two main parameters to define a spatial discretization, the "Tessellated U" (Tess U) and "Tessellated W" (Tess W), which determine, respectively, the number of divisions in relation to the radius and the chord of the rotor, to build the 3D geometry and vortex lattice mesh.

To evaluate the spatial discretization convergence, ten combinations of parameters, presented in Table 4.3, were analysed. To define these combinations, disproportional elements were avoided, trying to keep the elements close to a square shape, as is shown in Figure 4.3, where the mesh 9x40 is not desired, due to the elongated elements highlighted in red. Also, in Figure 4.3 is shown a blade with a low (25x40) and a high (57x80) degree of discretization.

This analysis was performed using the simulation parameters shown in the Table 4.4. The advance ratio (J) was chosen as 0.525 to avoid the non-linear aerodynamic effects. The proportional time-step (Δt^*) is the angle that the propeller rotates in one time-step (Δt), as defined in equation 10. Furthermore, the aerodynamic results are the temporal average of the forces and coefficients, ignoring the first rotation to avoid the transient effects.

$$\Delta t^* = \Delta t \frac{RPM}{60} 360 \tag{10}$$

Both aerodynamic and acoustic models were considered to evaluate the mesh convergence. For the aerodynamic results, the parameter used for the analysis was the thrust force.

This was chosen over the thrust coefficient because it is easier to understand the influence of variation on a physical quantity than a dimensionless coefficient. For the acoustic analysis, the overall sound pressure level was observed for three virtual microphones, positioned on an arc perpendicular to the rotor plane. The arc has a radius of 1.905 meters and is centered in the propeller center. The microphones are placed at angles of 0°, 22.5°, and 45° below the plan of the rotor, as illustrated in the Figure 4.4.

The results are shown in Figure 4.5 (a). Looking at the thrust force, it is possible to infer that the convergence is obtained from discretization 5 (57x80), since the results do not vary much after this point on. A slight step is observed for the mesh 8 (65 x 80) because it is the discretization where the Tess W parameter was increased (OpenVSP has some predefined values for Tess W and does not allow defining any value, as is the case with Tess U), however, this step varies below 2%, which represents a difference of 0.015 N, a tolerable error. In addition, the computational time spent on each analysis is presented in Figure 4.5 (b), where a quadratic behavior is observed, but a reduction of the time simulation can be seen for mesh 8 (65x80), due to a discretization with fewer elements than the previous one. Observing these values and relating them with thrust force convergence, it is possible to highlight meshes 5 (57x80) and 8 (65x80) as good options.

For acoustic convergence analysis, the OASPL of the three microphones is plotted in the Figure 4.6 for thickness, loading, and total noise. The reference pressure used for the sound pressure level was $2 \times 10^{-5} Pa$. For the total noise, the difference between the maximum and minimum values for each microphone (0°, 22.5°, and 45° respectively) is 0.7452 dB, 0.7189 dB, and 0.6577 dB, indicating a low mesh dependency. The same behavior is observed for thickness and loading noise, where from the mesh 4 (49x70) the results are almost constant for thickness noise and the difference with the average value is less than 0.2 dB for loading noise.

In this way, mashes with a refinement degree greater than mesh 5 (57x80) are converged for aerodynamics and acoustics analyses.

Table 4.3: Meshes used for spatial discretization convergence.

	Tess W	Tess U
1	25	40
2	33	50
3	41	60
4	49	70
5	57	80
6	57	90
7	57	100
8	65	80
9	65	90
10	65	100

Source: Own authorship.

Table 4.4: Simulation parameters for spatial discretization analysis.

Rotation speed	4003 *RPM*
J	0.525
Free-stream velocity	9.79 m/s
Total number of rotations	4
Proportional time-step	3°
Air density	1.225 kg/m^3
Kinematic viscosity	$1.516 \times 10^{-5} m^2/s$

Source: Own authorship.

Figure 4.3: The upper image illustrates the discretization avoided, with the elongated elements, as is highlighted in red. The images at the middle and bottom show the meshes with a low and high degree of discretization, respectively.

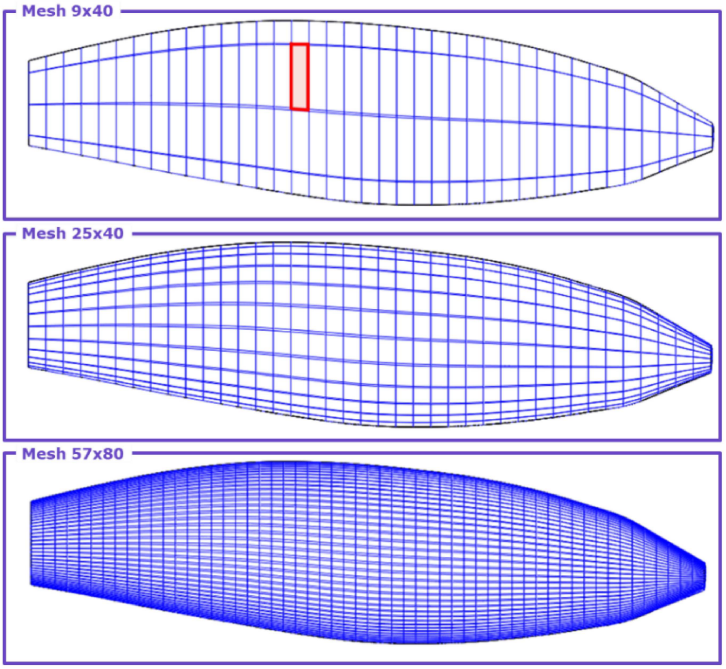

Source: Own authorship.

Figure 4.4: Positioning of virtual microphones for acoustic analyses.

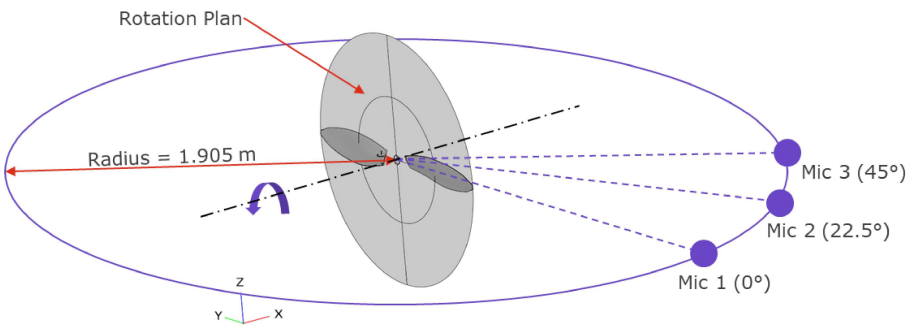

Source: Own authorship.

Figure 4.5: Convergence of thrust force (a) and total simulation time (b) for spatial discretization.

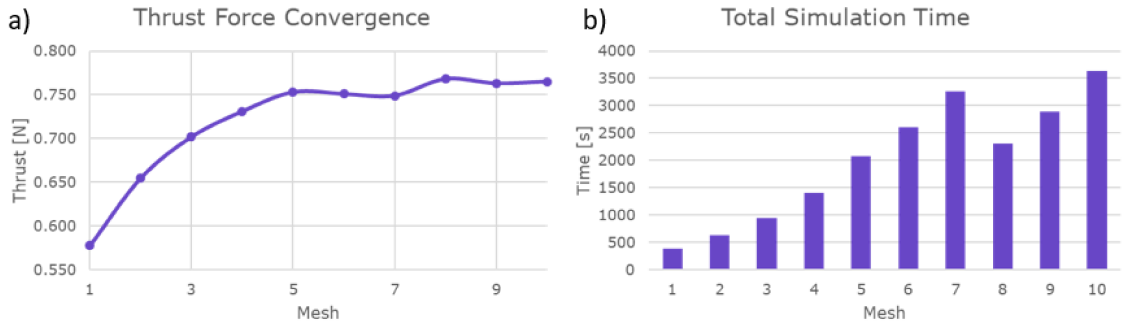

Source: Own authorship.

Figure 4.6: Convergence of overall sound pressure level for thickness noise (a), loading noise (b), and total noise (c) as a function of spatial discretization.

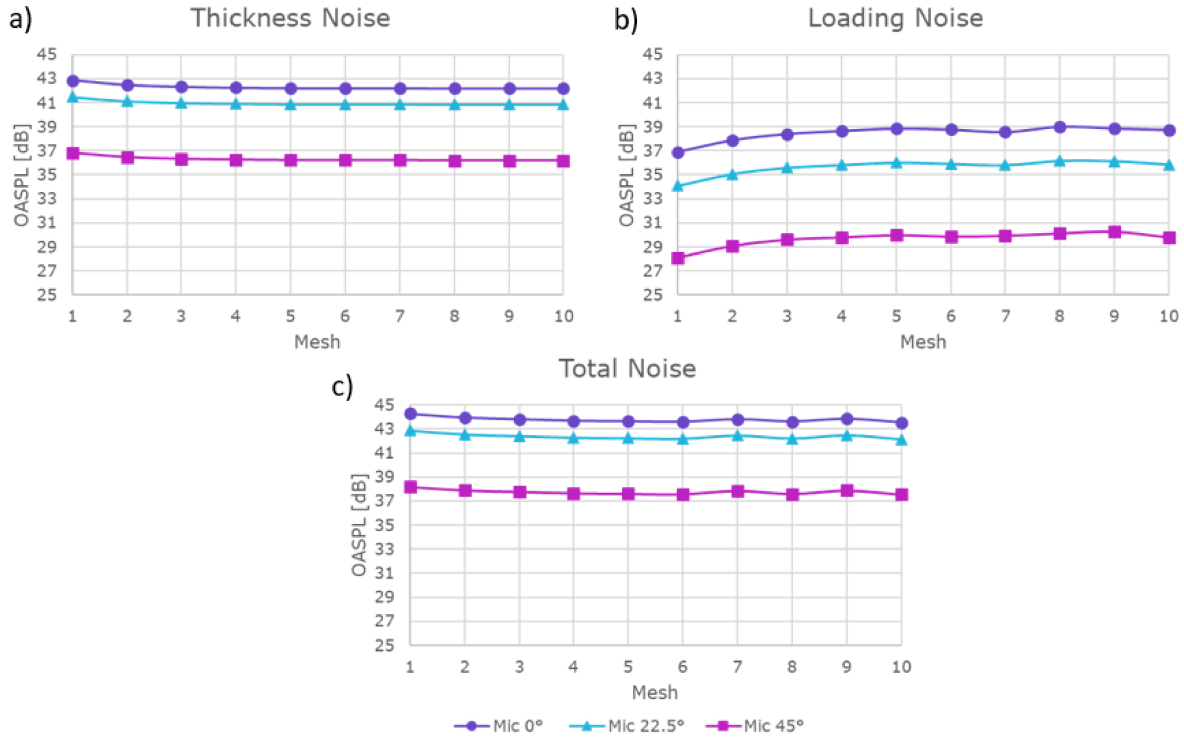

Source: Own authorship.

4.4 TEMPORAL DISCRETIZATION CONVERGENCE

To study the convergence of temporal discretization, simulations with a proportional time-step to 3°, 5°, 8°, 10°, 15°, 18°, 20° were performed for the aerodynamic and acoustic models. The proportional time-step is the angle that the propeller rotates in one time-step, as defined by equation 10. The conditions for the simulation were the same as spatial discretization

convergence and mesh 8 (65x80) was used. The proportional time-step less than 3° was not calculated because OpenVSP has problems to export the acoustics files.

Figure 4.7 shows the thrust force extracted from aerodynamic analysis, where it is possible to observe that the values fluctuate around the average, but for the time-step of 3°, the thrust tends to increase. Despite the fluctuations, the variation is less than 0.01 N, which denotes a low dependence of the aerodynamic model with the time-step. This is because the results are averaged over time, and increase the time-step makes the results more widespread, increasing the standard deviation, but keeping the temporal average almost equal.

The acoustic results are presented in Figure 4.8. In it, it is possible to observe that the thickness noise is not impacted by the time-step, as it depends only on spatial discretization. For loading noise, and as a consequence of total noise, the overall sound pressure level does not vary much between a time-step of 3° and 10°, but afterward, an increasing trend is observed. This is related to the loading vectors exported from OpenVSP and inputted into PSU-WOPWOP, which are less accurate with large time-steps.

To respect the convergence for both models, it is interesting to keep the proportional time-step below 10°.

Figure 4.7: Influence of proportional time-step on thrust force.

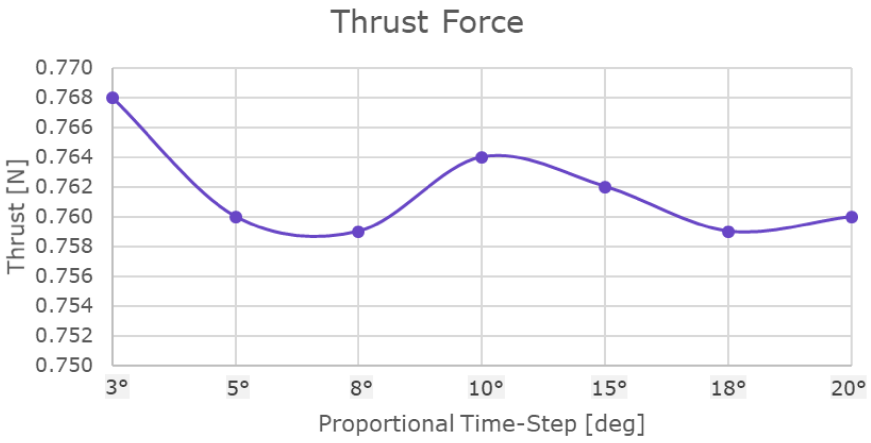

Source: Own authorship.

Figure 4.8: Influence of proportional time-step on acoustic results. Thickness noise (a), loading noise (b), and total noise (c).

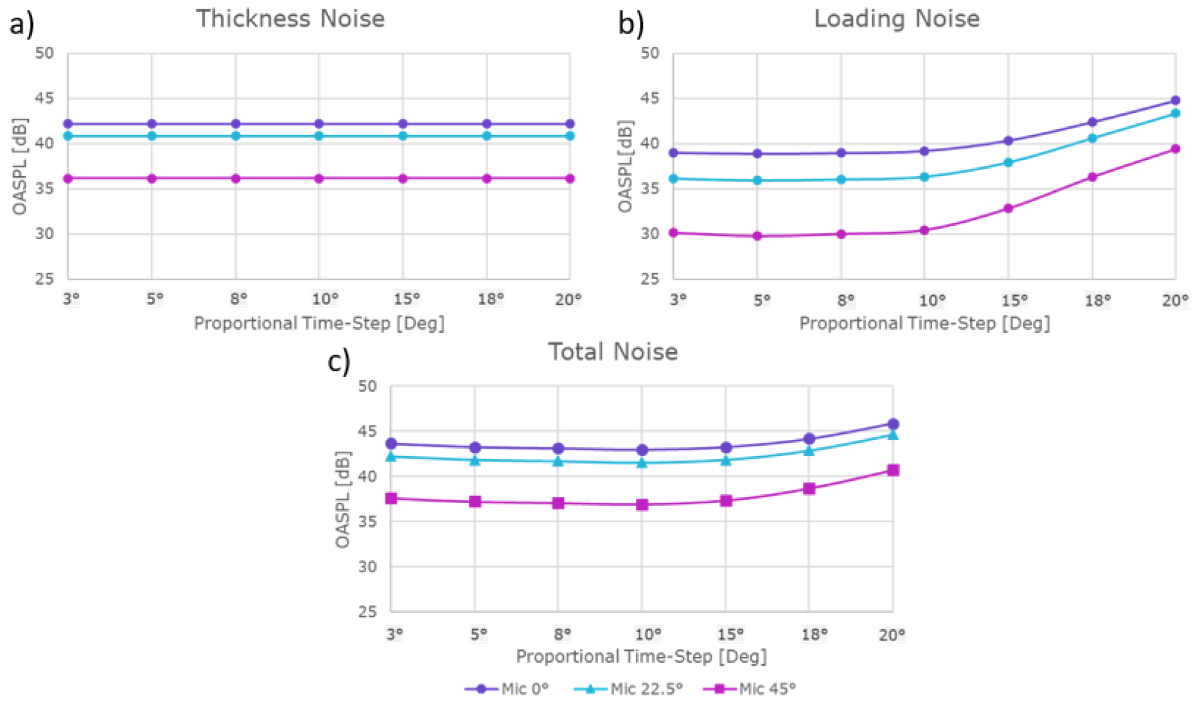

Source: Own authorship.

4.5 TOTAL NUMBER OF REVOLUTIONS

To evaluate the influence of a total number of revolutions analyzed, a study considering the same conditions of the temporal discretization convergence was carried out, but here varying the number total of revolutions from 3 to 10 and considering a proportional time step of 3°.

A weak influence was observed for the aerodynamic and acoustic results, presenting a difference in the order of 10^{-4}. This is due to the temporal average being calculate neglecting the first rotation, where the transient effects are observed. Furthermore, a refined spatial and temporal discretization was used, and perhaps with less refinement, a greater influence would be observed, but this hypothesis was not verified.

4.6 AERODYNAMIC VALIDATION

The aerodynamic validation was performed based on the propeller APC 11x4.7 SF, whose geometry is described in section 4.1. The thrust coefficient calculated using OpenVSP and VSPAERO was compared with the experimental data extracted from [13], where the performance coefficients for this propeller were obtained from wind tunnel experiments. Thus, the

rotation speed was kept constant and the free-stream velocity was varied. The same procedure was performed for different rotation speeds.

The same flow conditions of the experiments were defined in the OpenVSP model. In addition, the other parameters used for this simulation are shown in Table 4.5. Three rotation speeds were considered: 3004 RPM, 4003 RPM, and 5003 RPM, chosen according to the data available.

Figure 4.9 shows the thrust coefficient obtained with OpenVSP and the experimental data. Comparing both, it is possible to see that the OpenVSP results are well correlated with experimental data between an advance ratio of 0.30 and 0.60. Outside this range, the numeric solver overestimates the thrust coefficient. For an advance ratio greater than 0.6 this overprediction is subtle, but for an advance ratio less than 0.3 this is more severe. This same behavior is observed for the three rotation speeds rotation cases.

A hypothesis of why this effect occurs can be found by looking at how the angle of attack varies with the free-stream velocity variation for a constant speed rotation, as is schematized in Figure 4.10. When the free-stream velocity vector ($\vec{v}$) is reduced, the advance ratio is reduced and the γ angle tends also to decrease to respect the vector sum, which increases the angle of attack (α). On the other hand, when the free-stream velocity is increased, the angle of attack decreases. It depends on the blade twist, but for some low advance ratio, it is possible to find regions with a high angle of attack, where non-linear aerodynamic effects may exist. Likewise, when the free-stream velocity is high, the angle of attack is weak, and non-linear effects may also be present. As the VLM is a linear method, the non-linear effects are not captured, and the consequence is the lack of correlation between the experimental and numeric data.

This aerodynamic validation was performed for a propeller designed for a slow fly condition. Thus, in other cases, the valid advance ratio range can change depending on geometric parameters of the blade, mainly the twist angle. It is also important to note that the solver does not present satisfactory results for low free-stream velocity values, which prevents an accurate result for some fly conditions, such as the static case in a hover flight. Furthermore, the VSPAERO does not converge for static cases without flow.

Table 4.5: Parameter of simulation for aerodynamic validation.

Mesh	$57x90$
Rotation speed	3004,4003,5003 RPM
Total number of revolutions	4
Total number of rotations for average	3
Proportional time-step	3°
Air density	$1.225\ kg/m^3$
Kinematic viscosity	$1.516 \times 10^{-5} m^2/s$

Source: Own authorship.

Figure 4.9: Thrust coefficient for APC 11x4.7 SF calculated with OpenVSP for different rotation speeds.

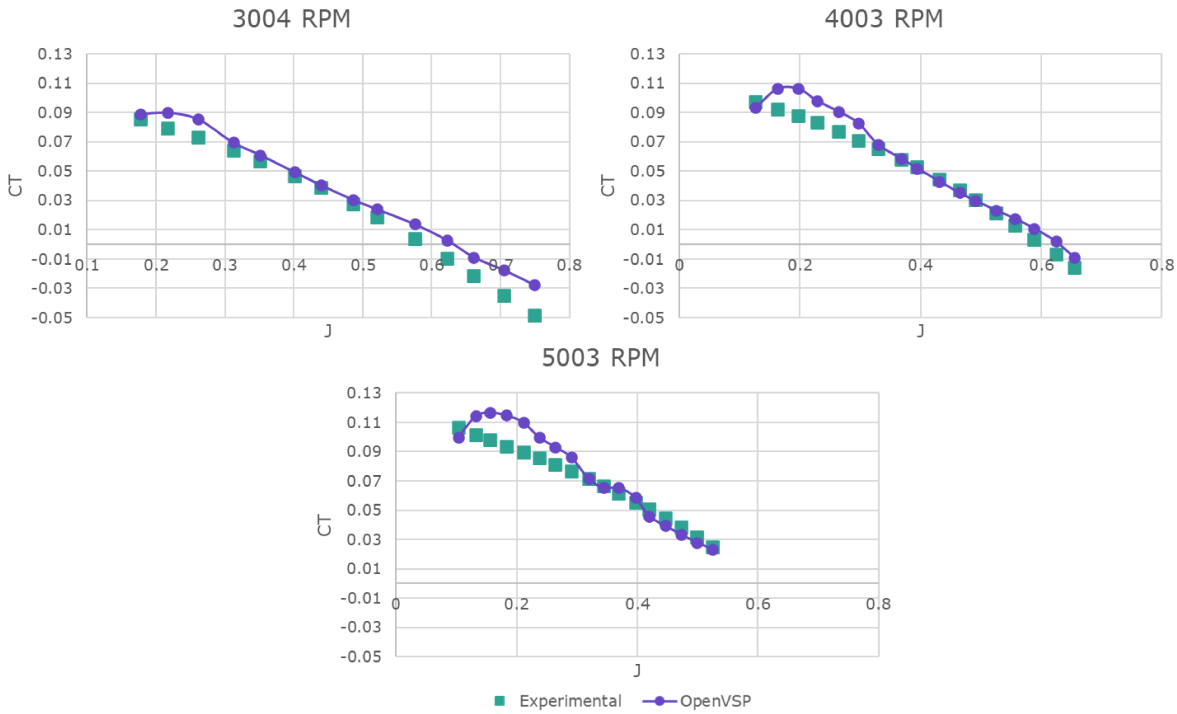

Source: Own authorship.

Figure 4.10: Influence of free-stream velocity on propeller angle of attack.

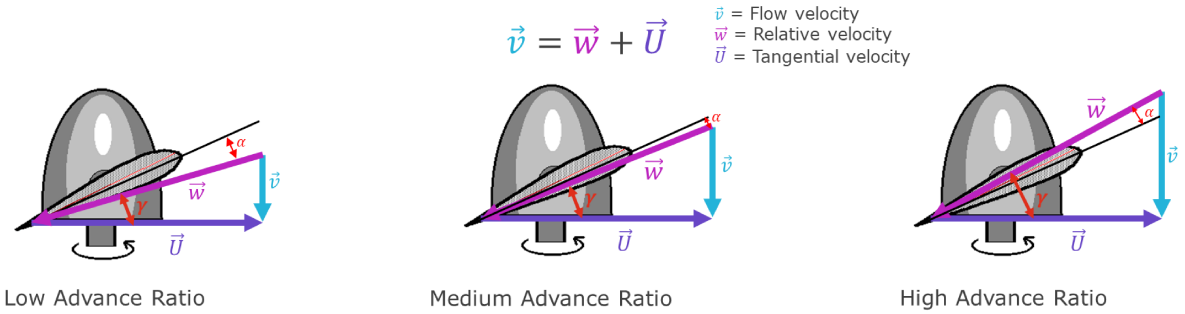

Source: Own authorship.

4.7 AEROACOUSTIC VALIDATION

With the aim of study the validity of the aeroacoustics model, the noise radiated by the propeller APC 11x4.7 SF was evaluated, and the results were compared with the experimental and numerical data available in [4]. For this procedure, nine virtual microphones were placed in an arc perpendicular to the rotation plan, as is shown in Figure 4.11, with them positioned from 90° above the rotor plan to -90° below it, with a step of 22.5°. The arc radius was set to 1.905 meters to match with the experiments and to ensure a microphone in a far-field region.

Figure 4.11: Positioning of virtual microphones for the aeroacoustic validation study. The negative angles are associated with the region below the rotor.

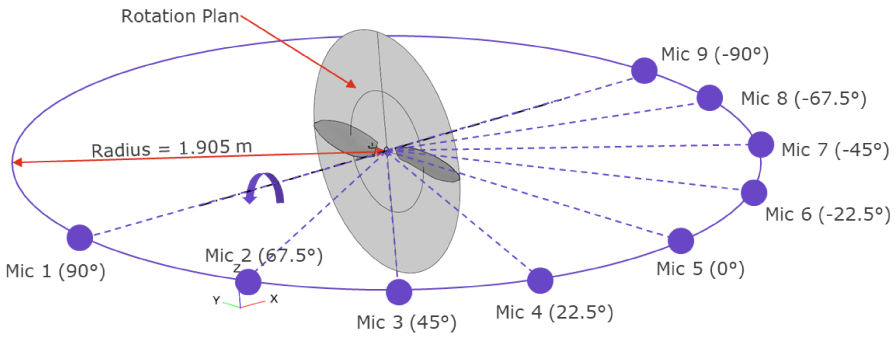

Source: Own authorship.

The rotation speeds chosen for this analysis were the same as those of the experiments: 3600 RPM, 4200 RPM, and 4800 RPM. As a result, the sound pressure level (SPL) spectrum and the overall sound pressure level were obtained. The PSU-WOPWOP was configured to calculate a frequency range between 100 Hz and 20 kHz with a resolution of 5 Hz. This resolution was chosen equal to the experimental data and also to avoid the influence of numerical instabilities. The reference pressure for acoustic calculation was defined as $20 \times 10^{-5} Pa$.

For aerodynamic sources, the data obtained from OpenVSP were used, where the simulation parameters are presented in Table 4.6. The experiments were performed in an anechoic chamber without a flow, however, OpenVSP is not able to predict the aerodynamic results in this condition, so, a free-stream velocity was set in order to obtain an advance ratio of 0.30, following the conclusions of the section 4.6.

Table 4.6: Aerodynamic calculation parameters for aeroacoustics validation analysis.

Mesh	65x80
Rotation Speed	3600,4200,4800 RPM
Free-stream velocity	5.02,5.86,6.70 m/s
Advance ratio	0.30, 0.30, 0.30
Total number of revolutions	4
Total number of rotations for average	3
Proportional Time-Step	4°
Air density	$1.225\ kg/m^3$
Kinematic Viscosity	$1.516 \times 10^{-5} m^2/s$

Source: Own authorship.

As explained in the bibliography review, only the thickness and loading noise are predicted, both deterministic sources with periodic behavior. The tonal frequency of the rotors, also known as blade passage frequency (BPF), is associated with the rotation speed and the number of blades, as defined in [Eq. 11].

$$BPF = \frac{RPM}{60} \times \text{N}^\circ \text{ of blades} \tag{11}$$

For this propeller, with two blades and rotation speed of 3600 RPM, 4200 RPM, and 4800 RPM, the blade passage frequency is respectively 120 Hz, 140 Hz, and 160 Hz. Figure 4.12 shows a SPL spectrum of a microphone 7 (-45°) for the three rotation speed cases. Firstly, the spectrum is composed of a sequence of peaks, which represents the blade passage frequency and the respective harmonics (multiple frequencies of the BPF). The blade passage frequency is determined by the first peak and the SPL is higher at this frequency than the others. In all three cases, the BPF is well captured and the value is the same as theoretically predicted. Secondly, the SPL between the peaks are low, due to the non-modeling of broadband noise.

Figure 4.13, extracted from [4], shows the SPL spectrum for the microphone positioned 45° below the rotor for the 4200 RPM case. Comparing the results with experimental data, it is possible to see that in the experimental spectrum a motor is present and contributes to the SPL, especially after 500 Hz, where it becomes an important acoustic source. As the motor is not considered in the calculations, this same effect is not observed in the PSU-WOPWOP simulations. Besides that, the SPL for the blade passage frequency is a little higher in the experiments, with a difference of 1.82 dB. Also, the SPL has a tendency to decrease for frequencies greater than 10 kHz, and the same behavior is observed for PSU-WOPWOP results. In general terms, the SPL predicted by the numerical method is lower than that observed in the experiment, but they have similar behavior, disregarding the contribution of the motor. The reason why the SPL is underestimated by the simulations can be related to the acoustic sources considered, where only the thickness and loading noise are predicted, but in the experiment other sources are present. Furthermore, the aerodynamic simulation was performed for a dynamic case with a free-stream velocity, unlike the experiment, which reduces the aerodynamic load and, as consequence, the contribution of loading noise to the total noise.

Figure 4.12: Sound pressure level spectrum for propeller APC 11x4.7 SF.

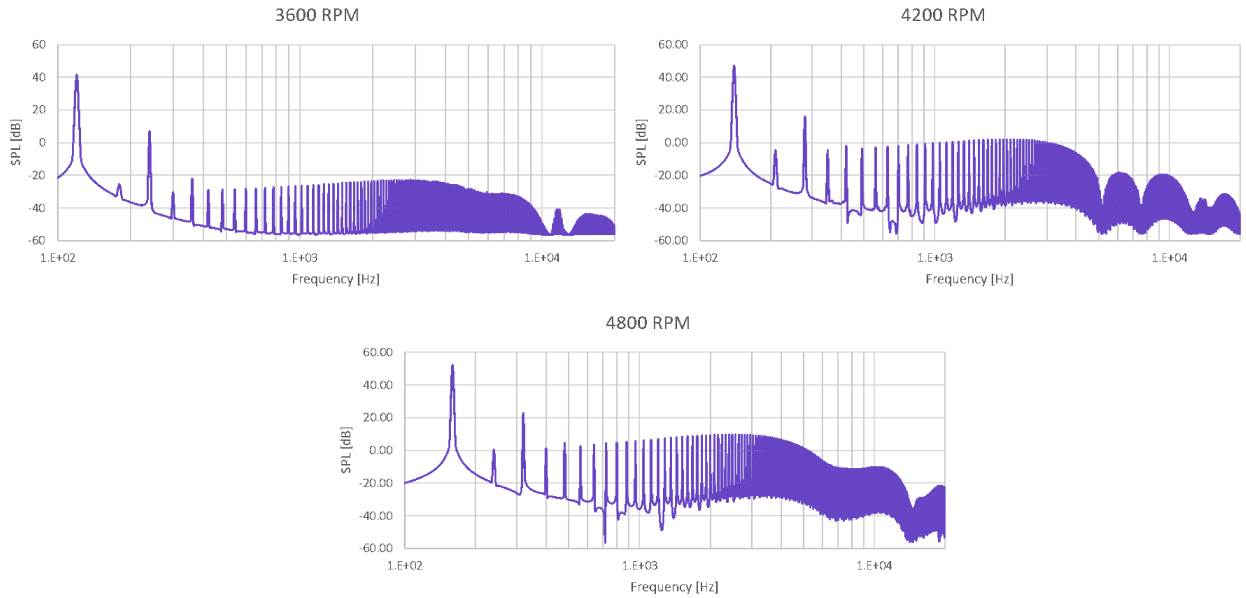

Source: Own authorship.

Figure 4.13: Experimental sound pressure level spectrum for propeller APC 11x4.7 SF.

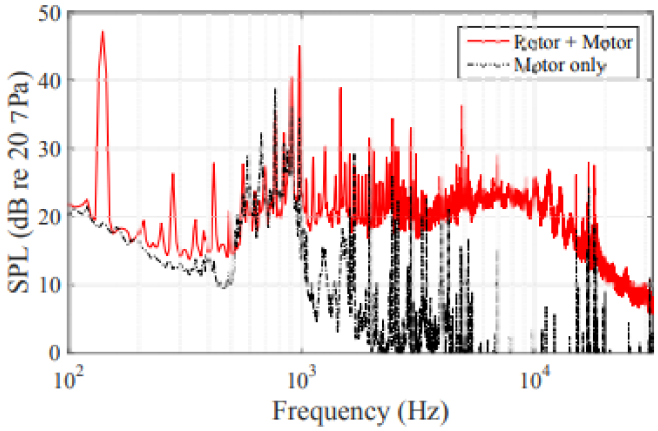

(a) APC-SF rotor, $\Omega = 4200$ RPM

Source: N. S. Zawodny, D. D. Boyd, and C. Burley [4]

A study of sound directivity was performed and, for this, the overall sound pressure level was organized in a polar graph, showing the contributions of thickness, loading for a total noise. The results for the 4200 RPM case are shown in Figure 4.14 (a). As expected, the thickness noise radiation is maximum when the microphone is aligned with the rotation plan and minimum when aligned with the axis of rotation. The same behavior is observed for a loading noise, but this source is dominant close to the axis of rotation. The total noise is the superposition of both sources.

Directivity for total noise was compared with the experimental data, as is shown in Figure 4.14 (b). The numerical results are not correlated with experimental values and the

error is relatively large. The receiver at 0° presents the smallest error, 4.40 dB, already a high difference. In addition, the shape of the curves is not similar. This can happen because, in the experiment, noise sources with different directivity characteristics are existents, such as the motor noise, which can be a dominant source for some directions where propeller noise becomes less important, like near to the axis of rotation. To verify this hypothesis, the directivity can be observed considering the sound pressure level for the blade passage frequency, because the noise generated by the blades is dominant over other sources. Figure 4.15 presents this comparison for the three rotation speeds. It is possible to notice that the results for the acoustic model are well correlated with the experimental values, having a similar shape and trend. The biggest error is 2.85 dB for a -45° position at 4800 RPM, an acceptable error. The Table 4.7 presents the error for each receiver.

Considering all the observations about the acoustic method, it is possible to notice that the solver predicts the sound pressure level at the blade passage frequency well, but the overall sound pressure level is underestimated.

Table 4.7: Absolute error for directivity of sound pressure level at blade passage frequency.

Receiver	3600 RPM	4200 RPM	4800 RPM
45.0°	1.99 *dB*	1.11 *dB*	1.26 *dB*
22.5°	1.45 *dB*	0.58 *dB*	0.67 *dB*
0.0°	1.48 *dB*	0.08 *dB*	1.14 *dB*
-22.5°	1.56 *dB*	0.91 *dB*	1.34 *dB*
-45.0°	0.27 *dB*	1.82 *dB*	2.35 *dB*

Source: Own authorship.

Figure 4.14: Directivity of noise radiated by thickness, loading, and total noise (a). Comparison between total noise calculated by PSU-WOPWOP and experimental results (b).

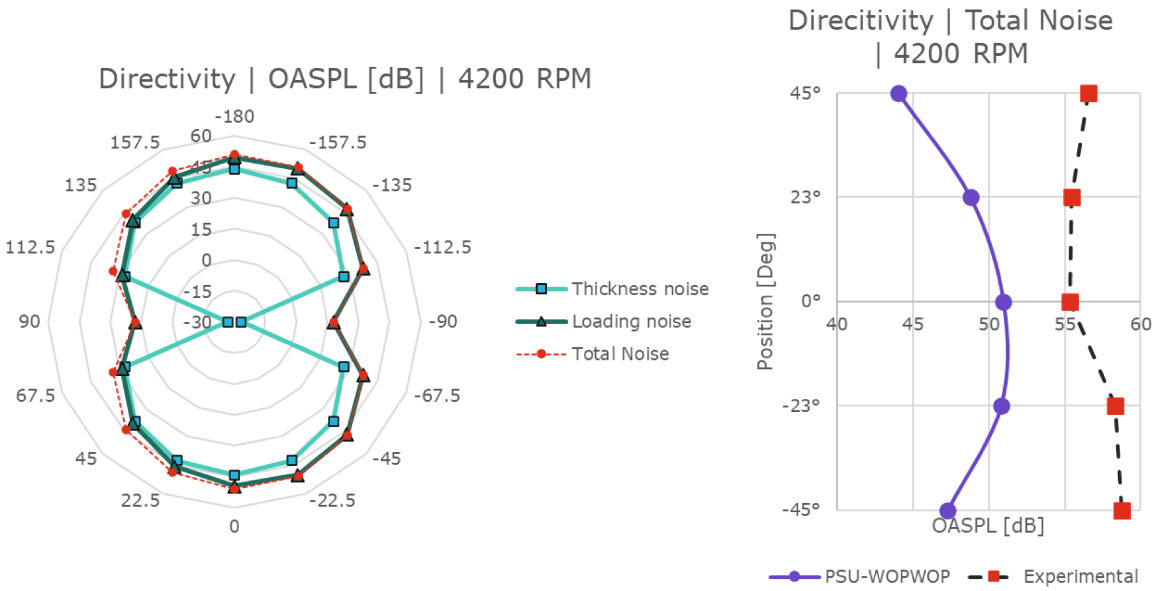

Source: Own authorship.

Figure 4.15: Directivity for sound pressure level at blade passage frequency for the three rotation speeds.

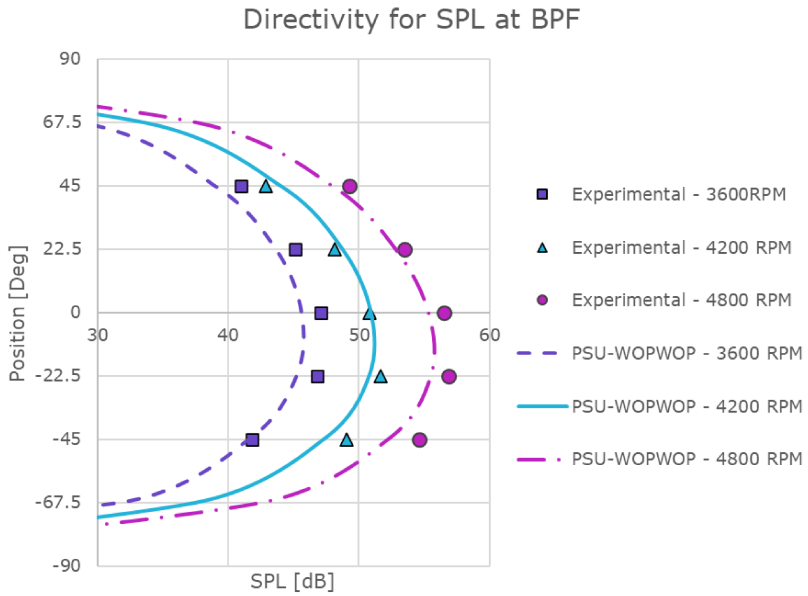

Source: Own authorship.

4.8 OPTIMIZATION CASE

An optimization case was performed to test the methodology and bugs in the script. As the objective was to test the algorithm, a simple case was performed, and the results presented here do not represent an optimization cycle valid for a propeller design. The propeller APC 11x4.7 SF was used as the base geometry.

The target of the optimization was the airfoil distribution along the blades. For this purpose, a NACA-4 digit airfoil was defined in three blade positions, at the hub, at $r/R = 0.5$, and at the tip. For this class of airfoils, four numbers are present in the nomenclature, like in NACA-4412. The first number indicates the maximum camber, the second the distance of maximum camber from the airfoil leading edge and the last two digits the maximum thickness, all as a percentage of the chord. In the example, the NACA-4412 has a maximum camber of 4% positioned at 40% of the chord and a maximum thickness of 12%.

Thus, in the optimization the maximum camber position was kept constant and equal to 40% and the camber and thickness were varied. As is not possible change directly the camber value in OpenVSP, the design lift coefficient (CLi) distribution was varied, producing a similar effect. Even if the thickness effects are neglected by the VLM, this was considered because it impacts the noise estimation. The simulations conditions used are presented in Table 4.8 as well the interval for the optimization variables.

Table 4.8: Simulation conditions and intervals of the variables for the optimization case.

Mesh	65x80
Free-stream velocity	8.00 m/s
Total number of revolutions	2
Total number of rotations for average	1
Proportional time-step	10°
Lower rotation speed	4000 *RPM*
Top rotation speed	5000 *RPM*
Thrust required	1.20 N
Air density	1.225 kg/m^3
Kinematic viscosity	1.516×10^{-5} m^2/s
Thickness hub (min, max)	(0.05, 0.13)
Thickness $r/R = 0.5$ (min, max)	(0.03, 0.10)
Thickness tip (min, max)	(0.03, 0.10)
CLi hub (min, max)	(0.50, 0.80)
CLi $r/R = 0.5$ (min, max)	(0.30, 0.95)
CLi tip (min, max)	(0.30, 0.80)

Source: Own authorship.

As objective function, the overall sound pressure level for a total noise observed by a receiver at a distance of 1.905 meters from the propeller and placed at 45° below the rotor was defined. The best geometry of the cycle is presented in Table 4.9, it is possible to notice some parameters are closer to the interval limits, and the execution of another cycle changing the limits is interesting. The aeroacoustics results for this geometry are compared with the original APC 11x4.7 SF, as presented in Table 4.10. As conclusion, the total noise was reduced from 53.04 dB to 38.93 dB, for an iso-thrust case, and the sound pressure level at blade passage frequency decreases 7.83 dB. The rotation speed to the iso-thrust condition increased 636 RPM, which reflect in a variation of 15 Hz on BPF.

Table 4.9: Geometry of the optimization result.

Thickness hub	0.0581
Thickness $r/R = 0.5$	0.0309
Thickness tip	0.0346
CLi hub	0.7792
CLi $r/R = 0.5$	0.3899
CLi tip	0.5313
Airfoil hub	NACA-6406
Airfoil $r/R = 0.5$	NACA-3403
Airfoil tip	NACA-4403

Source: Own authorship.

Table 4.10: Comparison between the performance of APC 11x4.7 SF and the optimized propeller.

	APC 11x4.7 SF	Optimized	Difference
Speed rotation	4200 *RPM*	4636 *RPM*	+636 *RPM*
Trust	1.20 *N*	1.24 *N*	+0.04 *N* (3.3%)
CT	0.040	0.035	-0.005
CQ	0.0034	0.0026	-0.0008
$OASPL_{thickness}$	37.88 *dB*	33.18 *dB*	-4.70 *dB*
$OASPL_{loading}$	52.87 *dB*	41.33 *dB*	-11.54 *dB*
$OASPL_{total}$	53.04 *dB*	38.93 *dB*	-14.11 *dB*
SPL_{BPF}	44.92 *dB*	37.09 *dB*	-7.83 *dB*
BPF	140 Hz	155 Hz	+15 Hz

Source: Own authorship.

5 CONCLUSIONS

This work was carried out to develop, study and validate a methodology for propellers aeroacoustic prediction. Observing the results, the aerodynamic model showed a good correlation with experimental data, however, it was limited for a range of advance ratio, where outside this interval the results are not well correlated. Because of this, the simulation of the hover condition is not possible. Despite that, the model is interesting because for valid conditions the results are good. In addition, it is also possible to perform unsteady calculations with a computational cost much lower than a CFD. The good correlation of the aerodynamic results can also be limited by the Reynolds number. For the propellers smaller than APC 11x4,7 SF, the Reynolds number tends to be smaller as well, and the VLM can calculate a result that is less corelated with the reality based on the observations made on section 3.3.

Looking at the acoustic results, the model well predicts the sound pressure level at the blade passage frequency, as well as the sound directivity for this parameter. For the entire sound spectrum, the solver does not predict the SPL very well for the higher frequencies. This is due to dominant acoustic sources other than thickness and loading for these frequencies, which are not modeled here. As a consequence, the overall sound pressure level is underestimated. Thus, the methodology using OpenVSP and PSU-WOPWOP has some limitations, but this is still an interesting tool to perform quick analyses in order to compare the acoustic and aerodynamic performance of different propellers.

Although the calculation time is shorter compared to a hybrid acoustic method based on CFD calculation, this is still not enough for a good calculation performance in an optimization process. For the case performed, the average time for each geometry was close to 280 seconds, which made the process last four days. Thus, the use of low-fidelity steady methods (such as BEMT) seems a better option to execute optimization cycles, using the methodology developed here as a tool to check and validate the results.

In this study, only the propeller geometry was considered to perform the aeroacoustics analyses. However, for the next steps of the work, it is interesting to consider the structures of the drone to verify the influence on acoustic radiation. For this, experiments and numerical simulations with the entire drone can be performed. Furthermore, is interesting to simulate the APC 11x4.7 SF and the geometry optimized using a high-fidelity method to check if the acoustic gain obtained with the optimization is observed using a method more accurate. Finally, it is interesting also to test the methodology presented in a real propeller project, where specifications and requirements must be respected.

REFERENCES

[1] M. J. Lighthill, "On sound generated aerodynamically i. general theory," *Proceedings of the Royal Society of London. Series A. Mathematical and Physical Sciences*, vol. 211, no. 1107, pp. 564–587, 1952.

[2] J. E. Ffowcs Williams and D. L. Hawkings, "Sound generation by turbulence and surfaces in arbitrary motion," *Philosophical Transactions of the Royal Society of London. Series A, Mathematical and Physical Sciences*, vol. 264, no. 1151, pp. 321–342, 1969.

[3] F. Farassat and G. P. Succi, "The prediction of helicopter rotor discrete frequency noise," in *American Helicopter Society, Annual Forum*, 1982, pp. 497–507.

[4] N. S. Zawodny, D. D. Boyd, and C. Burley, "Acoustic characterization and prediction of representative, small-scale rotary-wing unmanned aircraft system components," in *American Helicopter Society 72nd Annual Forum Proceedings*, 2016.

[5] K. S. Brentner and F. Farassat, "Modeling aerodynamically generated sound of helicopter rotors," *Progress in Aerospace Sciences*, vol. 39, no. 2, pp. 83–120, 2003.

[6] R. K. Amiet, *Noise produced by turbulent flow into a rotor: Theory manual for noise calculation*, Final Report United Technologies Research Center, 1989.

[7] T. Brooks and C. Burley, "Blade wake interaction noise for a main rotor," *Journal of the American Helicopter Society*, vol. 49, pp. 11–27, 2004.

[8] T. Brooks, D. Pope, and M. Marcolini, *Airfoil self-noise and prediction*, NASA RP 1218, 1989.

[9] C. Burley and T. Brooks, "Rotor broadband noise prediction with comparison to model data," *Journal of the American Helicopter Society*, vol. 49, pp. 28–42, 2001.

[10] C. C. Hennes, L. V. Lopes, J. Shirey, *et al.*, *Psu-wopwop 3.4.4 user's guide*, The Pennsylvania State University, 2021.

[11] R. J. Pegg, *A summary and evaluation of semi-empirical methods for the prediction of helicopter rotor noise*, NASA Technical Memorandum 80200, 1979.

[12] J. Brandt and M. Selig, "Propeller performance data at low reynolds numbers," *49th AIAA Aerospace Sciences Meeting*, 2011.

[13] J. Brandt, R. W. Deters, G. K. Ananda, O. D. Dantsker, and M. Selig, *Uiuc propeller data site*, `https://m-selig.ae.illinois.edu/props/propDB.html`.

[14] Y. Jo, T. Jardin, R. Gojon, M. Jacob, and J.-M. Moschetta, "Prediction of noise from low reynolds number rotors with different number of blades using a non-linear vortex lattice method," in *25th AIAA/CEAS Aeroacoustics Conference*, 2019, pp. 1–13.

[15] C. Nana, J.-M. Moschetta, E. Benard, S. Prothin, and T. Jardin, "Experimental and numerical analysis of quiet mav rotors," in *50th 3AF International Conference*, 2015.

[16] R. Serré, V. Chapin, J.-M. Moschetta, and H. Fournier, “Reducing the noise of micro-air vehicles in hover,” in *International Micro Air Vehicle Conference and Flight Competition (IMAV 2017)*, 2017, pp. 51–59.

[17] J. Jordaan, “Acoustic meta-atoms: An experimental determination of the monopole and dipole scattering coefficients,” Ph.D. dissertation, 2017.

[18] S. Glegg and W. Devenport, *Aeroacoustics of Low Mach Number Flows*. Elsevier Science, 2017.